6th European Conference on Computational Mechanics (ECCM 6)
7th European Conference on Computational Fluid Dynamics (ECFD 7)
1115 June 2018, Glasgow, UK

COMPARATIVE STUDY OF THE PREDICTION OF HIGH ANGLE OF ATTACK PHENOMENA USING TRANSITIONAL TURBULENCE MODELS

JOLAN WAUTERS[1], JORIS DEGROOTE[1,2] AND JAN VIERENDEELS[1,2]

[1] Department of Flow, Heat and Combustion Mechanics, Ghent University
Sint-Pietersnieuwstraat 41, 9000, Ghent, Belgium
email: jolan.wauters, joris.degroote, jan.vierendeels@ugent.be

[2] EEDT, Flanders Make

Key words: low Reynolds flow, stall cell, transitional turbulence models, laminar separation bubble, high amplitude low frequency oscillation

Abstract. In this paper transitional turbulence modeling is approached from the point of view relevant to small unmanned aerial vehicles (span $\approx 1m$), of which the flow is characterized by very low values of turbulent intensity and transition is predominantly of the separation induced kind. Four different turbulence models for low Reynolds number flow will be used to predict the flow over a NACA 0018 profile in 3D for different geometric settings: infinite wing, finite wing clamped on one side and finite wing clamped on both sides. The latter two mimicking wind tunnel experiments. The turbulence models under consideration are Menter's $k-\omega$ SST model with Wilcox's low-Re modification, Menter & Langtry's $\gamma - Re_\theta$ model, it's simplified γ model and Walters & Cokljat's $k - k_l - \omega$ model. The NACA 0018 profile is placed in a flow with chord-based Reynolds number of 3×10^5 at an angle of attack (AoA) of 17^o, allowing an assessment of the prediction of high angle of attack related phenomena, such as stall cells and high amplitude low frequency oscillations by means of URANS simulations.

1 INTRODUCTION

The applicability of unmanned aerial vehicles (UAVs) for military, humanitarian, commercial and recreational purposes has led to a large body of research in UAV-related fields. A deep understanding and correct modeling of the aerodynamic behavior is fundamental with the objective of further extending the capabilities of these UAVs. Here we focus on those that operate at a chord-based Reynolds numbers (Re_c) below 5×10^5, the condition which is referred to as *low Reynolds number flow* [1].

A characteristic of UAVs operating at low Reynolds numbers is the appearance of a separation bubble on the wing, also attributed to the low turbulence intensity of the external flow. It is fundamental in the analysis, design and optimization of the flight

behavior of UAVs to correctly model this phenomenon. This paper focuses on Reynolds-Averaged Navier-Stokes (RANS) simulations, which have obtained a more prominent role through their ability to be used in increasingly complex 3D geometries with a relatively low computational cost. Classic turbulence models, which serve to close the system of RANS equations, assume a fully turbulent flow. This makes their use in low Reynolds application somewhat ambiguous. The last couple of decades have however seen the birth of a number of turbulence models that attempt to model the transition phenomena.

Based on the manner by which transition is predicted, transitional turbulence models can be categorized as low Reynolds models, which make use of damping functions, correlation based models, which typically relate the production of intermittency to correlations depending on flow parameters, and physics-based models, which attempt to model the flow based on a more theoretical framework. Of the three categories, representatives are selected that are compared with each other to assess their abilities. Menter's $k-\omega$ Shear Stress Transport (SST) model [2] with Wilcox's low Reynolds modification [3] (henceforth referred to as the low-Re model) is taken as representative of the low Reynolds models. Menter and Langtry's $\gamma - Re_\theta$ model [4, 5] and Menter and Langtry's γ model [6] are taken as representatives of the correlation models. Walter & Cockljat's $k - k_l - \omega$ model [7] is taken as representative of the physics-based models.

Typically, the characteristics of an airfoil using RANS are assessed in 2D. This simplification can be justified for fully turbulent attached flows where the flow component in the third dimension is predominantly caused by turbulence and thus modelled. However, in the case of separation-induced transition, the third dimension becomes much more significant since the separation-induced transition process is characterized by the three-dimensional deformation of Kelvin Helmholtz billows and the vortex shedding from the bubble. The three-dimensionality of the flow is even more dominantly present at high angles of attack (AoAs), where experimental measurements have shown the appearance of stall cells (SCs) and/or high-amplitude low-frequency oscillations (HALFOs).

Stall cells (Figure 1) is the term in literature attributed to the experimentally [8, 9, 10, 11, 12, 13, 14, 15] and numerically [10, 15, 16] observed coherent structures characterized by a strong three dimensional nature of the wake near stall. They appear in the shape of counter-rotating swirl patterns, sometimes also poetically addressed as *owl faces* or *mushroom cells*, through the use of oil flow and tuft measurements. These structures appear in pairs and typically extend spanwise twice the length of the chord. When the span increases beyond AR=2, the cells get stretched before splitting and forming a new pair. The presence of stall cells results in an increased C_L compared to a fully 2D flow and translates itself in a reduced decrease of C_L for an AoA above the one corresponding to $C_{L,max}$, limited to a small region of $\approx 3^o$.

On the other hand, a number of studies [8, 17] observed a more violent fluctuating behavior of C_L in the corresponding AoA-region, attributed to shear-layer flapping [18]. They found that in the presence of a separation bubble, in time-averaged sense, the flow is two-dimensional and the stall cells are absent altogether. The flow is further more characterized by high-amplitude low-frequency oscillations and referred to as such.

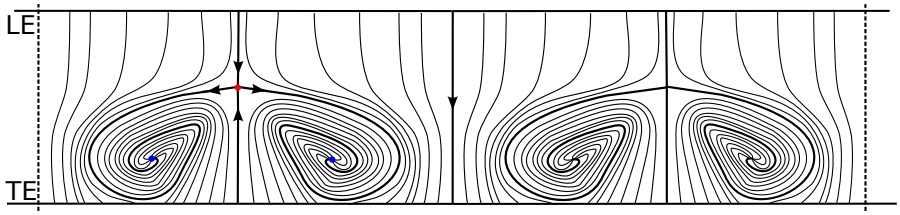

Figure 1: Schematic representation of the skin friction lines on the suction side of a section of a wing ($AR = 4$) confined by two symmetry planes (dotted lines) at an angle of attack just past the stall angle. The two stall cells are visible in the shape of counter rotating swirl patterns: two foci (blue dots) connected by a global separation line emerging from the saddle point (red dot).

The four turbulence models under consideration are compared for their ability to predict high AoA related phenomena in a low Reynolds flow in three different configurations: an infinite wing, a finite wing clamped on one side and a finite wing clamped on both sides through a series of URANS simulations.

2 METHODOLOGY

The URANS simulations are performed in such a way that they mimic the experimental measurements of a NACA 0018 profile performed by Timmer [19] for $Re_c = 3 \times 10^5$. The measurements were executed in the Delft University Wind Tunnel using a $0.25\,m$ chord model at velocities ranging between $10\,m/s$ and $70\,m/s$ with respectively corresponding turbulence intensity (Tu) values of 0.02% and 0.07%. This results in $Tu = 0.04\%$ for $Re_c = 3 \times 10^5$. The NACA 0018, being a thick profile, would likely be characterized by the appearance of both SCs as HALFOs in the AoA past stall [8].

From experimental studies and the use of Tu-dependent trigger functions in the transition models, it can be noted that Tu is a dominant parameter. RANS modeling has been characterized by a decay of Tu especially for external flows, predominantly found in aeronautical applications. This decay of Tu is caused by the fact that only the destruction terms in the k and ω transport equations are active between inlet and leading edge. Spalart & Rumsey [20] recognized the relevance of turbulent decay and the difficulty in defining a reasonable combination of Tu_{inlet} and μ_t/μ that would yield acceptable results. They proposed for aeronautical applications the following relation: $\mu_t/\mu \approx 2 \times 10^{-7} \times Re_c$, which yields for $Re_c = 3 \times 10^5$ the following: $\mu_t/\mu = 0.06$. This results in $Tu_{inlet} \approx 0.23\%$ in order to predict the value of Tu at the inlet of the computational domain that one may obtain a $Tu = 0.04\%$ at the leading edge.

The computational domain surrounding the airfoil is c-shaped: extending 10 chord lengths in front, above and below the airfoil and 20 chord lengths behind it as presented in Figure 2a. Chordal grid discretization, spanwize grid discretization, wall normal expansion ratio, first cell size and time step size were subjected to an independence study. The results correspond to the strict requirements for the mesh as put forward by Langtry and Menter [4, 5, 6]: a maximum wall normal expansion ratio of 1.1 should be imposed on minimal 100

layers surrounding the airfoil to obtain a y^+ of maximum 1 near the stagnation point, on average 0.35, and 100 nodes are placed on the chord. The span is discretized in such a way that the AR of cells on the surface of the wing is on average equal to 1. All calculations are performed using second order upwind for convective terms, second order central for diffusive terms, gradient least squares cell based discretization and the SIMPLE pressure-velocity coupling. The time step size corresponds to 10^{-4}, following a in CFD validated *von Neumann* stability analysis, to properly resolve vortex shedding using a transient second order implicit formulation.

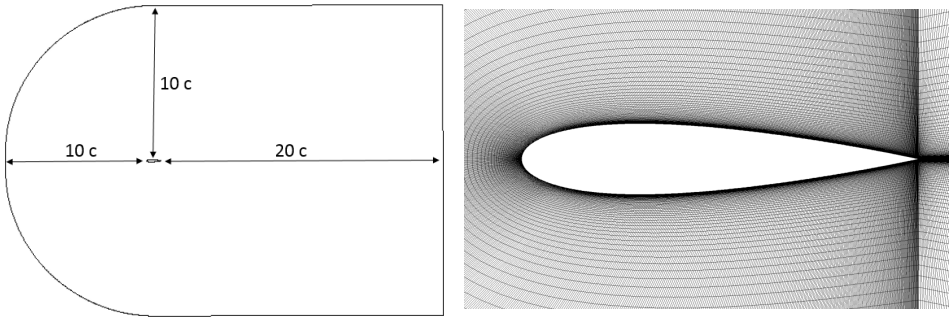

(a) Dimensions far-field

(b) Detail mesh resolution

Figure 2: Computational domain

In order to model an infinite wing in such a way that the SCs can be resolved, periodic boundary conditions at both ends are applied to a finite span with $s/c = 200\%$, resulting in 200 nodes along the span. This implies that the computational domain repeats itself an infinite number of times. For the wing clamped on one side, the computational domain is extended on one side with 10 chord-lengths to produce a free tip and closed with a symmetry boundary condition. On the side that the wing is clamped a no-slip boundary condition is imposed. For the third case, the wing clamped on both sides, the periodic boundary conditions of the first case are replaced by no slip boundaries, together with a velocity inlet and pressure outlet closing the computational domain.

The choice of AoA=17^o is based on the experimental observation of stall cells (SCs) and/or high-amplitude low-frequency oscillations (HALFOs) past the stall angle and before the burst angle, thus, according to Timmer's experimental measurements [19], possibly found at AoA=17^o.

3 RESULTS & DISCUSSION

To describe the three-dimensional separated flow field we make use of critical point theory [21] which allows us to assess the former based on a topographic description of the on-wall shear distribution. Contour plots of the suction side of the airfoil colored by instantaneous wall shear stress along with oil flow lines originating from 90% of the chord to some extent reproduce the results of the oil flow experiments. Discoloration

indicates the presence of vortex cores and movement of the oil flow towards the leading edge indicates the presence of flow separation.

3.1 Infinite Wing

The choice to examine an infinite wing comes forth from the statement by Weihs & Katz [12], who postulated that since a multitude of cells form when the AR is increased, the presence of tips or end-plates does not influence the formation of cells and that it is purely a product of the Crow instability: an interaction between two line vortices, here one originating from the leading edge and one from the trailing edge.

The low-Re model produces a spanwise uniform flow (Figure 3a), while the γ model clearly displays spanwise waviness of its separation front, unaffected by the vortex shedding from the separation bubble further upstream (note the discoloration spot near the leading edge of Figure 4a indicating the presence of vortex shedding of the separation bubble and the fairly continues separation front). The waviness corresponds to the initial phase of the crow instability, however there is no break up or formation of cells. Sarlak et al. [16] performed a URANS simulation on an infinite wing with S826 airfoil and observed a similar waviness in the separation front using the $k-\omega$ SST model. The $\gamma - Re_\theta$ model on the other hand is a prime example of violent vortex shedding from the separation bubble, breaking up the separation front, which results in a low frequency fluctuating flow (Figure 5a) with $St = O(10^{-2})$, roughly equal to experimental observations. As illustrated by Broeren & Bragg [8], the time average of the violent shedding flow is two-dimensional. This implies that if the spanwise size (s/c) is big enough to fully resolve the breakdown of the vortices, a further increase of the span should yield to the same averaged result. The opposite holds for stall cells, which will merge or split if s/c is changed. This results in a changing C_L caused by a jet effect between the cells. The fluctuations caused by the HALFOs increase with increasing AoA up to the point that the entire airfoil separates and behaves as a bluff body with $St = O(10^{-1})$. The $k-k_l-\omega$ model predicts an attached flow along with a violent vortex shedding from the laminar separation bubble (Figure 6a).

3.2 One Side Clamped Wing

One of the earliest studies on SCs were performed by Winkelmann [13] and Bippes [9] on a wing clamped on one side. The appearance of a free tip results in the formation of a tip vortex. For small ARs this leads to a reduced suction peak and consequently a delayed stall angle. On the side of the wall a horseshoe vortex appears caused by the interaction of the wall boundary layer and wing boundary layer.

The low-Re model produces a separation front that disappears near the tip and curls up near the end-plate (Figure 3b), producing as it were half of a stall cell. As opposed to the infinite wing, the separation front has progressed far less towards the leading edge, conform the statement above, yet again steady in time. The discoloration near the tip illustrates the presence of the tip vortex. The γ model produces a similar trend (Figure 4b), however the wavefront has extend further. The $\gamma - Re_\theta$ model again shows a distorted wavefront

caused by vortices shed from the laminar separation bubble (Figure 5b). Anew we see for the $k - k_l - \omega$ model a vortex shedding from the separation bubble, but no separation originating from the trailing edge (Figure 6b).

3.3 Two Side Clamped Wing

A wing clamped on both sides, as typically encountered in wind tunnel experiments, is here fully resolved instead of imposing a symmetry condition on half the model as for example done by Zarutskaya & Arieli [15] and Manolesos et al. [10]. While justifiable in case of steady simulations, as performed by the aforementioned, unsteady measurements have shown the unsteady tendency of stall cells [14].

The low-Re model produces a clear stall cell, noticeable from the distinctive oil flow lines on the suction side (Figure 3c). The γ model shows a similar coherent structure, but asymmetric in nature: with a very low frequency $St = O(10^{-3})$ the eyes of the structure alternately growing and shrinking in nature (Figure 4c). The latter justifies the choice to resolve the entire span and not work with a symmetry condition as mentioned above, even though the time averaged flow field corresponds to the symmetric one. This results in large fluctuations in C_L: $\Delta C_L \approx 0.5$. Yon & Katz [14] found the appearance of both HALFOs as SCs, but found no correlation between them. They did however note that the SCs move in time, a phenomenon to which they referred as *'jostling'*. The $\gamma - Re_\theta$ model sees the appearance of the former superposed on the appearance of HALFOs discusses in Section 3.1 (Figure 5c). Ragni & Ferreira [11] experimentally measured the appearance of SCs in the presence of a separation bubble, but found that the latter had no influence on the formation of the former. The $k - k_l - \omega$ model again predicts a strongly attached flow subjected to a violent vortex shedding from the separation bubble (Figure 6c).

4 CONCLUSION

Four transitional turbulence models, Menter's $k - \omega$ SST model with Wilcox's low-Re modification, Menter & Langtry's ($k - \omega$ SST) $\gamma - Re_\theta$ model, it's simplified ($k - \omega$ SST) γ model and Walters & Cokljat's $k - k_l - \omega$ model, were compared for their ability to predict high AoA related coherent structures for three different geometric settings: an infinite wing, to asses the presence of the Crow instability, a one side clamped wing and a two side clamped wing to mimic the experimental oil flow measurements in a wind tunnel.

We found a different degree of separation for the different geometric settings for all four models, caused by the end-plates and/or free tips. While not a new results [22, 17], we stress the importance of considering the geometric setting of the experiment when comparing it 2D or 3D simulations.

Furthermore, it was found that the low-Re model predicts a steady flow in the three geometric settings, with a clear formation of a SC in case of a two-side clamped wing. The γ model predicts the waviness which preludes the crow instability as predicted by Weihs & Katz [12] in case of an infinite wing, but showed no breaking of the separation front. This might still occur at higher AoAs, but must be assessed in future research. In case of a two-side clamped wing it shows 'jostling' as experimentally observed by Yon &

Katz [14]. The $\gamma - Re_\theta$ model shows a similar behavior as the γ model, but with the appearance of a violent vortex shedding of the separation bubble, leading to HALFOs. The $k - k_l - \omega$, while capable of predicting the vortex shedding of the separation bubble, fails to predict a separation front originating from the trailing edge.

ACKNOWLEDGEMENTS

Conducted as part of the EUFORIA (Efficient Uncertainty quantification For Optimization in Robust design of Industrial Applications) project under the financial support of the IWT, the Flemish agency of Innovation through Science and Technology. This work was carried out using the STEVIN Supercomputer Infrastructure at Ghent University, funded by Ghent University, the Flemish Supercomputer Center (VSC), the Hercules Foundation and the Flemish Government department EWI.

REFERENCES

[1] Lissaman, P. B. S. "Low-Reynolds-Number Airfoils," *Annual Review of Fluid Mechanics* Vol. 15, No. 1, 1983, pp. 223-239.

[2] Menter, F. R. "Two-equation eddy-viscosity turbulence models for engineering applications," *AIAA Journal* Vol. 32, No. 8, 1994, pp. 1598-1605.

[3] Wilcox, D. A. "Simulation of Transition with a Two-Equation Turbulence Model," *AIAA Journal* Vol. 32, No. 2, 1994, pp. 247-255.

[4] Menter, F. R., Langtry, R. B., Likki, S. R., Suzen, Y. B., Huang, P. G., and Volker, S. "A correlation-based transition model using local variables - Part I: Model formulation," *Journal of Turbomachinery-Transactions of the ASME* Vol. 128, No. 3, 2006, pp. 413-422.

[5] Langtry, R. B., Menter, F. R., Likki, S. R., Suzen, Y. B., Huang, P. G., and Volker, S. "A correlation-based transition model using local variables - Part II: Test cases and industrial applications," *Journal of Turbomachinery-Transactions of the ASME* Vol. 128, No. 3, 2006, pp. 423-434.

[6] Menter, F. R., Smirnov, P. E., Liu, T., and Avancha, R. "A One-Equation Local Correlation-Based Transition Model," *Flow Turbulence and Combustion* Vol. 95, No. 4, 2015, pp. 583-619.

[7] Walters, D. K., and Cokljat, D. "A Three-Equation Eddy-Viscosity Model for Reynolds-Averaged Navier-Stokes Simulations of Transitional Flow," *Journal of Fluids Engineering-Transactions of the ASME* Vol. 130, No. 12, 2008, p. 14.

[8] Broeren, A. P., and Bragg, M. B. "Spanwise Variation in the Unsteady Stalling Flowfields of Two-Dimensional Airfoil Models," *AIAA Journal* Vol. 39, No. 9, 2001, pp. 1641-1651.

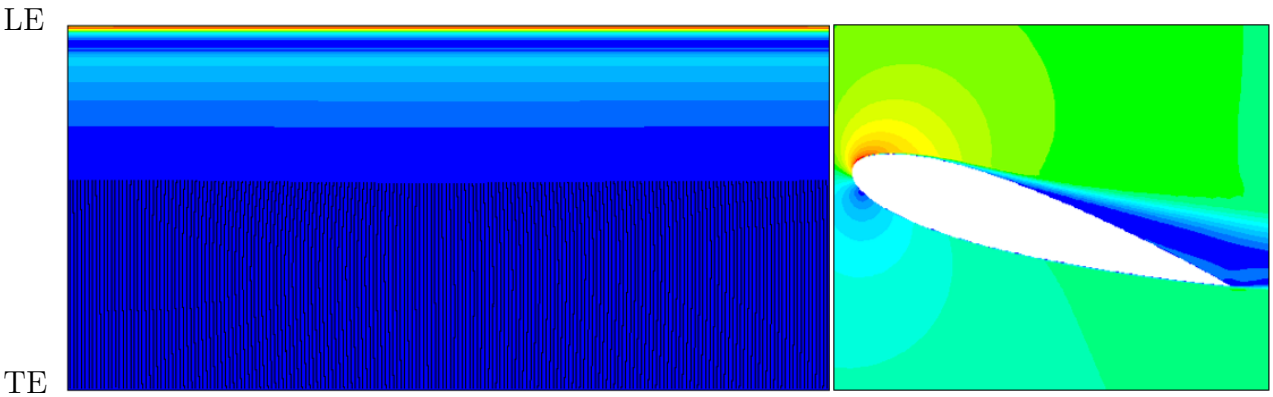

(a) Infinite wing

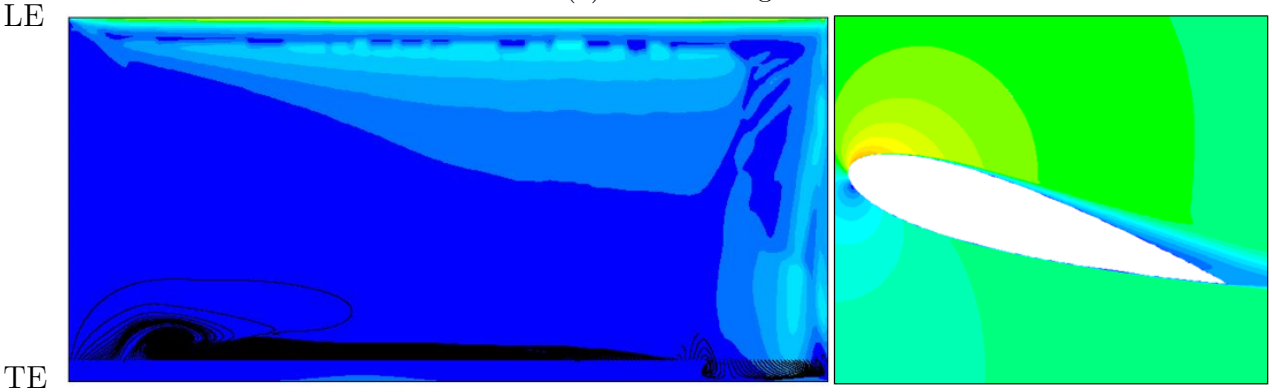

(b) Finite wing clamped on left side

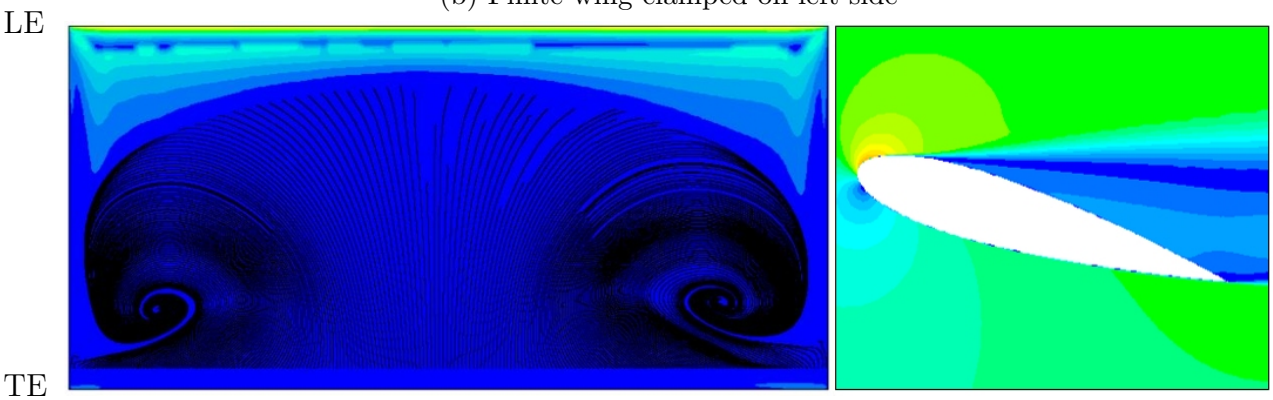

(c) Finite wing clamped on both sides

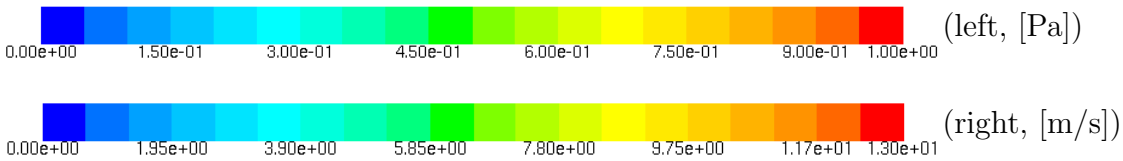

Figure 3: Contour plot of the instantaneous wall shear stress on the suction side with the leading edge at the top (LE) and the trailing edge at the bottom (TE) with oil flow pathlines originating from 90% of the chord (left) and contour plot of the instantaneous velocity magnitude of a cross-section at half the span (right) at AoA=17^o with $s/c = 200\%$ for the low-Re model.

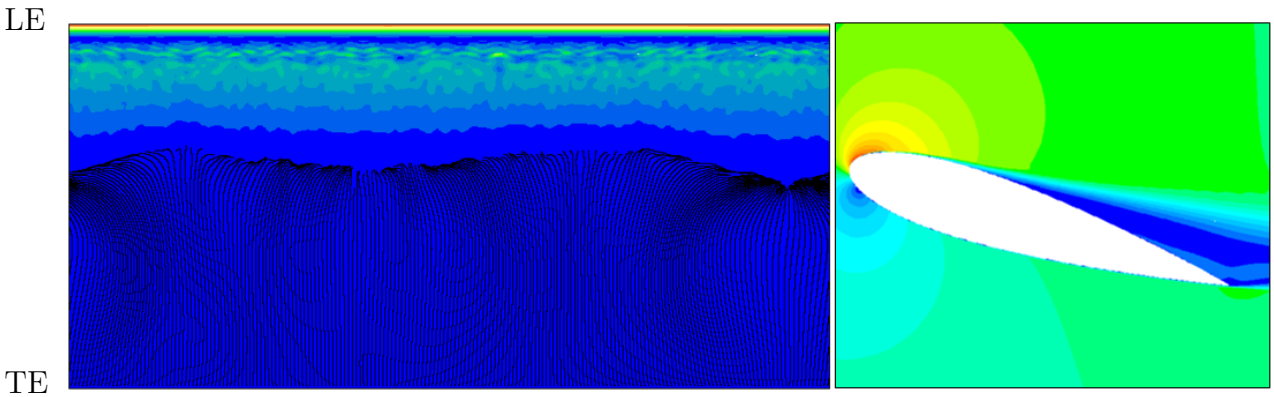

(a) Infinite wing

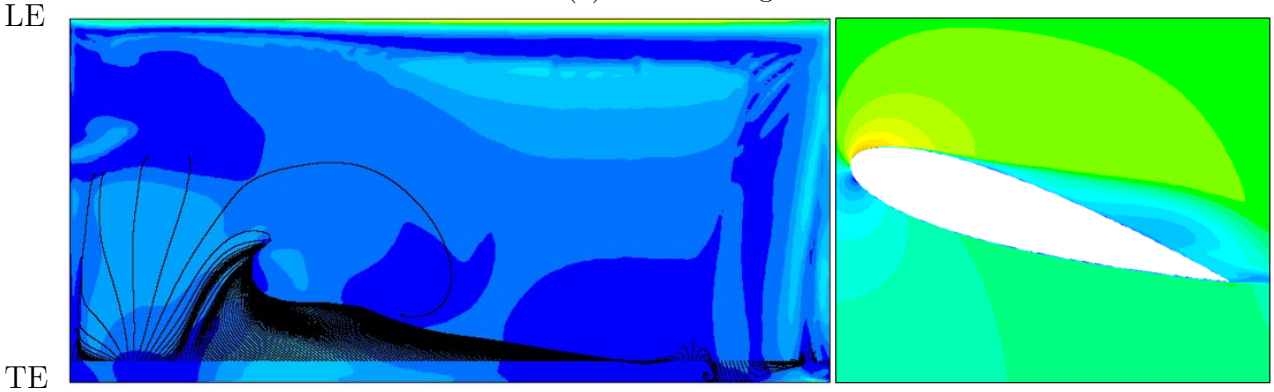

(b) Finite wing clamped on left side

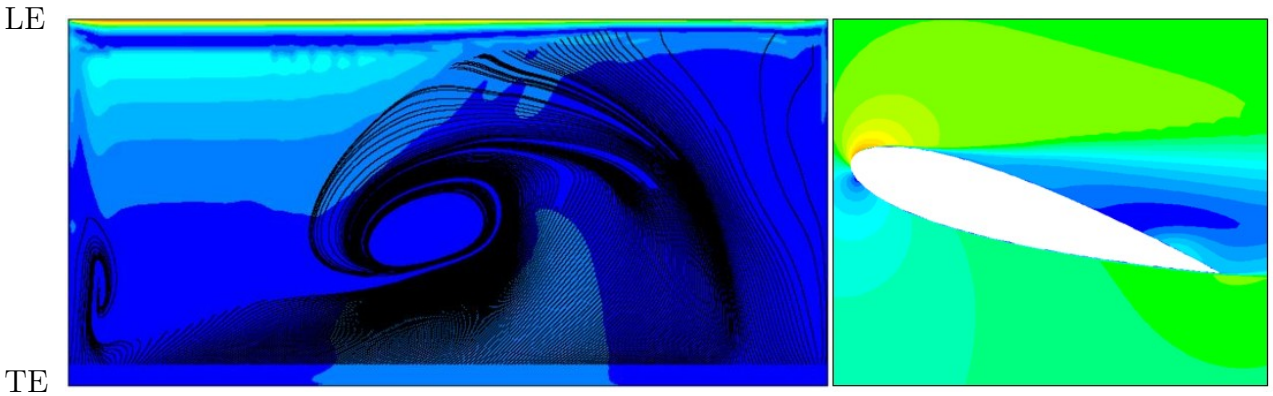

(c) Finite wing clamped on both sides

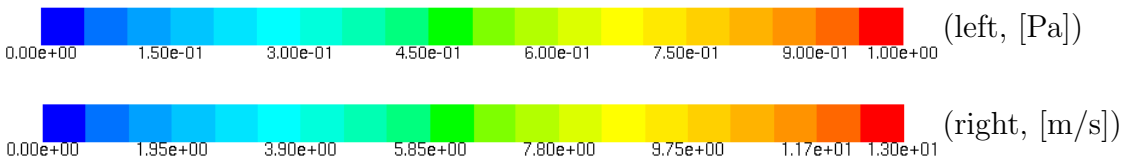

Figure 4: Contour plot of the instantaneous wall shear stress on the suction side with the leading edge at the top (LE) and the trailing edge at the bottom (TE) with oil flow pathlines originating from 90% of the chord (left) and contour plot of the instantaneous velocity magnitude of a cross-section at half the span (right) at AoA=17^o with $s/c = 200\%$ for the γ model.

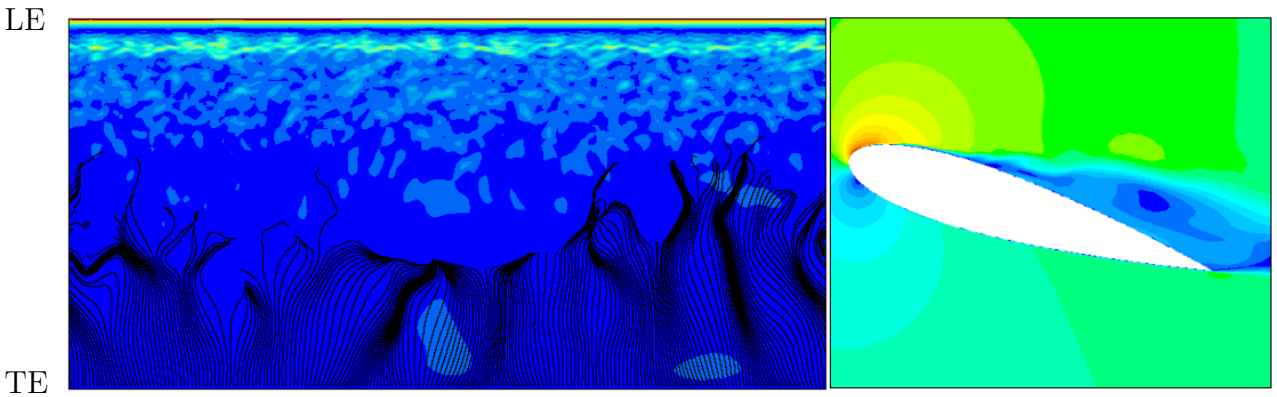

(a) Infinite wing

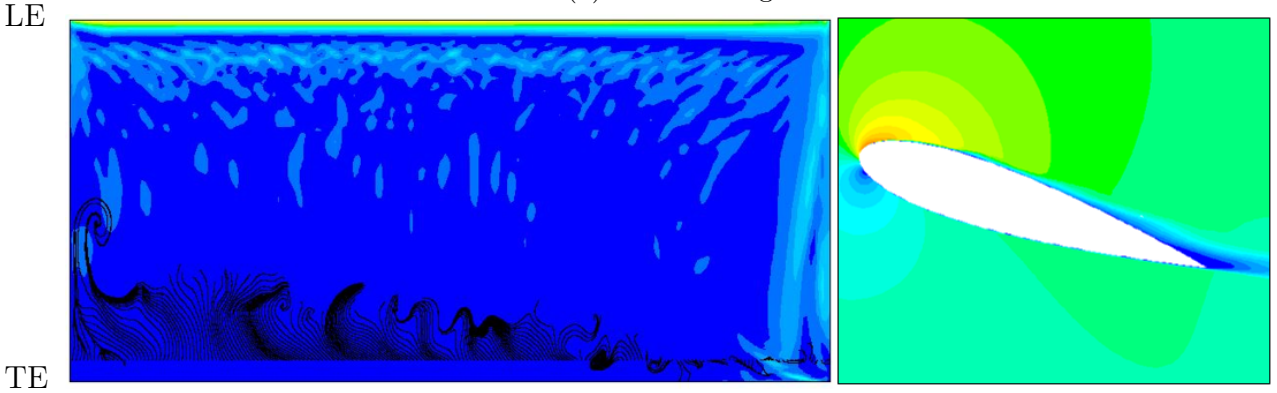

(b) Finite wing clamped on left side

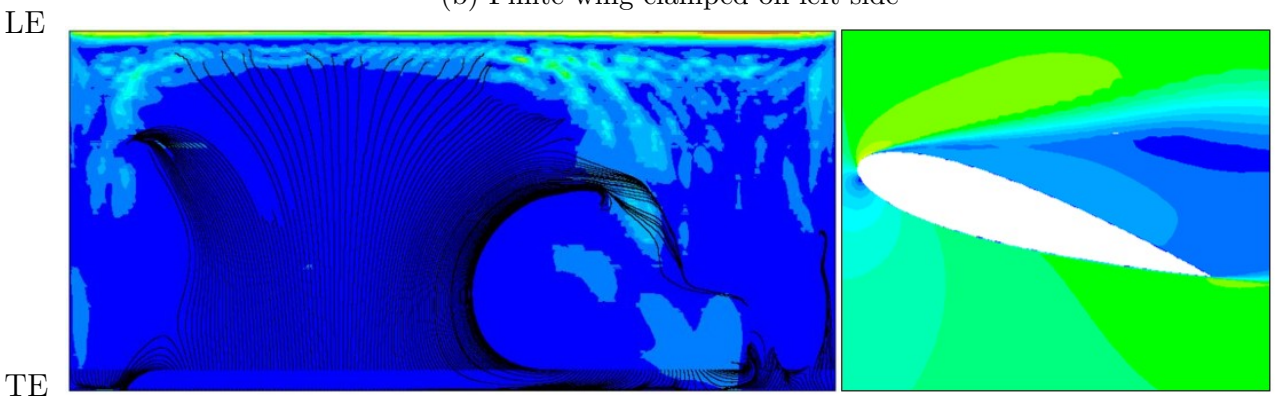

(c) Finite wing clamped on both sides

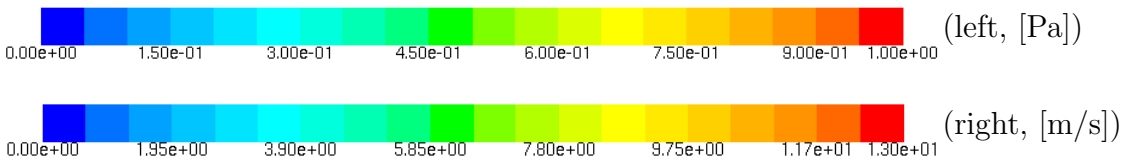

Figure 5: Contour plot of the instantaneous wall shear stress on the suction side with the leading edge at the top (LE) and the trailing edge at the bottom (TE) with oil flow pathlines originating from 90% of the chord (left) and contour plot of the instantaneous velocity magnitude of a cross-section at half the span (right) at AoA=17^o with $s/c = 200\%$ for the $\gamma - Re_\theta$ model.

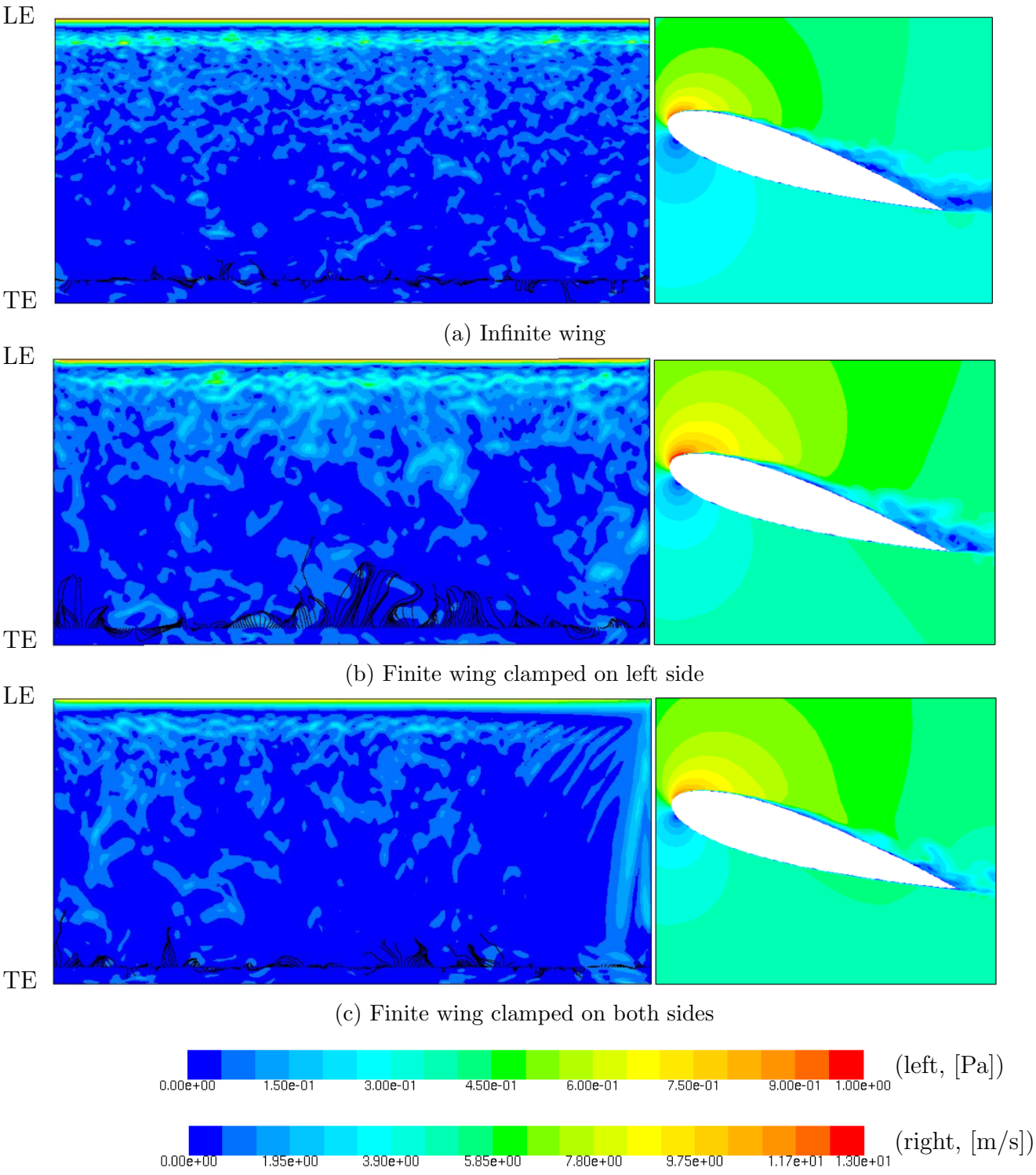

Figure 6: Contour plot of the instantaneous wall shear stress on the suction side with the leading edge at the top (LE) and the trailing edge at the bottom (TE) with oil flow pathlines originating from 90% of the chord (left) and contour plot of the instantaneous velocity magnitude of a cross-section at half the span (right) at AoA=17^o with $s/c = 200\%$ for the $k - k_l - \omega$ model.

[9] Bippes, H., and Turk, M. "Half Model Testing Applied to Wings above and below Stall," *Recent Contributions to Fluid Mechanics.* Springer Berlin Heidelberg, Berlin, Heidelberg, 1982, pp. 22-30.

[10] Manolesos, M., Papadakis, G., and Voutsinas, S. "An Experimental and Numerical Investigation on the Formation of Stall-Cells on Airfoils," *Journal of Physics: Conference Series* Vol. 555, 2012, pp. 012068 1-9.

[11] Ragni, D., and Ferreira, C. "Effect of 3D stall-cells on the pressure distribution of a laminar NACA64-418 wing," *Experiments in Fluids* Vol. 57, No. 8, 2016, p. 127.

[12] Weihs, D., and Katz, J. "Cellular patterns in poststall flow over unswept wings," *AIAA Journal* Vol. 21, No. 12, 1983, pp. 1757-1759.

[13] Winkelmann, A., Barlow, J., Saini, J., Anderson, J. J., and Jones, E. "The effects of leading edge modifications on the post-stall characteristics of wings," *18th Aerospace Sciences Meeting.* American Institute of Aeronautics and Astronautics, 1980.

[14] Yon, S. A., and Katz, J. "Study of the Unsteady Flow Features on a Stalled Wing," *AIAA Journal* Vol. 36, No. 3, 1998, pp. 305-312.

[15] Zarutskaya, T., and Arieli, R. "On Vortical Flow Structures at Wing Stall and Beyond," *35th AIAA Fluid Dynamics Conference and Exhibit.* American Institute of Aeronautics and Astronautics, 2005.

[16] Sarlak, H., Nishino, T., and Sorensen, J. N. "URANS simulations of separated flow with stall cells over an NREL S826 airfoil," *AIP Conference Proceedings* Vol. 1738, No. 1, 2016, p. 030039-1−030039-4.

[17] Bragg, M. B., Heinrich, D. C., and Khodadoust, A. "Low-Frequency Flow Oscillation over Airfoils near Stall," *AIAA Journal* Vol. 31, No. 7, 1993, pp. 1341-1343.

[18] Driver, D. M., Seegmiller, H. L., and Marvin, J. G. "Time-dependent behavior of a reattaching shear layer," *AIAA Journal* Vol. 25, No. 7, 1987, pp. 914-919.

[19] Timmer, W. A. "Two-Dimensional Low-Reynolds Number Wind Tunnel Results for Airfoil NACA 0018," *Wind Engineering* Vol. 32, No. 6, 2008, pp. 525-537.

[20] Spalart, P. R., and Rumsey, C. L. "Effective Inflow Conditions for Turbulence Models in Aerodynamic Calculations," *AIAA Journal* Vol. 45, No. 10, 2007, pp. 2544-2553.

[21] Délery, J. M. "Robert Legendre and Henri Werlé: Toward the Elucidation of Three-Dimensional Separation," *Annual Review of Fluid Mechanics* Vol. 33, No. 1, 2001, pp. 129-154.

[22] Pelletier, A., and Mueller, T. J. "Effect of endplates on two-dimensional airfoil testing at low Reynolds number," Journal of Aircraft Vol. 38, No. 6, 2001, pp. 1056-1059.